Ab initio study of the elastic properties of single and polycrystal TiO_2, ZrO_2 and HfO_2 in the cotunnite structure

2009 J. Phys.: Condens. Matter 21 015501

(http://iopscience.iop.org/0953-8984/21/1/015501)

J. Phys.: Condens. Matter **21** (2009) 015501 (11pp) doi:10.1088/0953-8984/21/1/015501

Ab initio study of the elastic properties of single and polycrystal TiO_2, ZrO_2 and HfO_2 in the cotunnite structure

M A Caravaca[1], J C Miño[1], V J Pérez[1], R A Casali[2] and C A Ponce[2]

[1] Departamento de Fisico-Quimica, Facultad de Ingenieria, UNNE, Avenida Las Heras 727, CP 3500, Resistencia, Argentina
[2] Departamento de Fisica, Facultad de Ciencias Exactas y Naturales y Agrimensura UNNE, Avenida Libertad 5600, CP 3400, Corrientes, Argentina

Received 17 April 2008, in final form 2 October 2008
Published 1 December 2008
Online at stacks.iop.org/JPhysCM/21/015501

Abstract

In this work, we study theoretically the elastic properties of the orthorhombic ($Pnma$) high-pressure phase of IV-B group oxides: titania, zirconia and hafnia. By means of the self-consistent SIESTA code, pseudopotentials, density functional theory in the LDA and GGA approximations, the total energies, hydrostatic pressures and stress tensor components are calculated. From the stress–strain relationships, in the linear regime, the elastic constants C_{ij} are determined. Derived elastic constants, such as bulk, Young's and shear modulus, Poisson coefficient and brittle/ductile behavior are estimated with the polycrystalline approach, using Voigt–Reuss–Hill theories. We have found that C_{11}, C_{22} and C_{33} elastic constants of hafnia and zirconia show increased strength with respect to the experimental values of the normal phase, $P2_1/c$. A similar situation applies to titania if these constants are compared with its normal phase, rutile. However, shear elastic constants C_{44}, C_{55} and C_{66} are similar to the values found in the normal phase. This fact increases the compound anisotropy as well as its ductile behavior. The dependence of unit-cell volumes under hydrostatic pressures is also analyzed. P–V data, fitted to third-order Birch–Murnaghan equations of state, provide the bulk modulus B_0 and its pressure derivatives B_0'. In this case, LDA estimations show good agreement with respect to recent measured bulk moduli of ZrO_2 and HfO_2.

Thermo-acoustic properties, e.g. the propagation speed of transverse, longitudinal elastic waves together with associated Debye temperatures, are also estimated.

1. Introduction

Oxides of group IV show a common group of properties such as corrosion resistance and high hardness. Their high dielectric constants make them potential material for the development of dielectric gates of sub-micrometer CMOS transistors.

On the other hand, the elastic properties are related to the fundamental quantities of the solid such as interatomic potentials, phonon spectra and equations of state, in addition to specific heat, thermal expansion, Debye temperature, melting point and Grüneisen parameters. The response of the crystal to external forces characterized by bulk modulus B, shear modulus G, Young's modulus E and Poisson's coefficient ν can be determined from the elastic constants C_{ij}. The ductile–brittle properties of materials are also closely related to the response to shear along slide planes, and is affected by the changes from contributions to the total energy caused by these deformations. The shear elastic constants C_{44}, C_{55} and C_{66} provide information regarding the bonding properties between adjacent planes of atoms and the anisotropic character of bonds. They are, therefore, useful in determining the structural stability of the crystal. Accurate experimental determinations of elastic constants need large pure single crystals which, in the case of many ceramics, are difficult to obtain. Thus *ab initio* theoretical studies which provide elastic properties of single and polycrystals are appropriate. A very important application is the knowledge of biaxial stresses caused by the epitaxial growth of thin films on a given substrate, as in the case of deposition of oxides, different to SiO_2, on silicon [100] wafers, used in the electronics industry. These stresses can be calculated by the knowledge of the biaxial elastic constants and heterostructure lattice mismatch. In the case of HfO_2, ZrO_2

and TiO_2 such *ab initio* calculations in the high density phase *Pnma* are scarce [1, 2] in the literature.

At room temperatures and at pressures above 30 GPa, zirconia and hafnia are transformed into an orthorhombic structure of cotunnite type named OII (spatial group *Pnma*) [3–11], which is quenched after decompression, with an equilibrium volume of 120.6 $Å^3$ and 118.6 $Å^3$, respectively [12]. Recently, it has been reported that a cotunnite structure in titanium oxide, currently the hardest naturally known oxide, has been obtained. This phase is synthesized at 48 GPa and 1900–2100 K with lattice parameters $a = 5.162$ Å, $b = 3.074$ Å and $c = 5.942$ Å, and a volume of 94.28 $Å^3$, and is one of the least compressible and toughest polycrystalline materials reported [13]. The aim of this work is to characterize the mechanical behavior represented by the elastic constants of the single-crystal *Pnma* phase. In order to compare the mechanical properties measured in ceramics of polycrystalline nature, we use Voigt–Reuss–Hill approximations [14–16].

In low symmetry systems, elastic constant calculations are scarce. This is due to the fact that, in addition to highly accurate methods able to evaluate small energy differences and/or the direct stress calculation, an appreciable number of small symmetry breaking distortions is required to determine a complete set of independent elastic constants. These, moreover, are increased as the system symmetry is reduced. In the cases therefore studied, with orthorhombic structure, there are a total of nine C_{ij}.

ZrO_2 and HfO_2 oxides are also currently investigated as dielectric or structural thin films, in which they are epitaxially grown over substrates such as metals or monocrystalline Si. In such a process, lattice mismatch can compromise the stability of the film. Therefore it is necessary to know the elastic constants beforehand, so that the film stresses due to biaxial deformations can be estimated.

2. Details of calculations

The SIESTA code [17] is used in this paper to calculate total energies, atomic forces and stresses solving the electronic quantum-mechanical equations using the density functional approach in the local density approximation (LDA) parametrized by Ceperley–Alder [18] and the generalized gradient approximation (GGA) of Perdew–Burke–Ernzerhof (PBE) [19]. The interaction between electrons and core ions are simulated through separable Troullier–Martins [20] norm-conserving pseudopotentials. The basis set is constructed with pseudoatomic orbitals (PAOs) of Sankey–Niklewski type, generalized to include multiple-zeta decays which are used to represent the valence wavefunctions.

We have generated the atomic pseudopotentials for the atoms entering in each compound. In the case of the Hf atom, we found that it is not necessary to include the Hf 4f shell in the valence set to achieve reliable results even in the more demanding case of the volume collapse of the cotunnite phase (the atomic volume decreases by 13%) (see [21, 22]). However, we found it is important to include partial core correction to Zr and Hf pseudopotential generation in order to find reliable equilibrium volumes with different basis sets. Thus, we have generated the atomic Zr pseudopotentials using the [Kr] $5s^2$ $4d^2$ atomic configuration and for Hf pseudopotentials the [Xe4f^{14}]$6s^2$ $5d^2$ atomic configuration. The cutoff radii selected for both atomic pseudopotentials were 2.7, 2.9 and 2.25 au for the s, p and d orbitals, respectively. For oxygen we have used 1.15 au for the s and p channels and 0.8 au for the d and f channels, respectively, and for Ti the 1.7, 1.6 and 1.6 au for the s, p and d channels, respectively. The Ti pseudo-atom is represented by a +2 ionized ion, in which valence set electrons are in a $3s^2$ $3p^6$ $3d^2$ configuration. This set together with an added channel of $4s^2$ electrons provide 12 electrons in the compound's electronic structure. In order to improve simplicity and efficiency, these pseudopotentials are transformed according to the methodology prescribed by Kleinman–Bylander [23] (see [21, 22]). To obtain the elastic constants, the equilibrium structural parameters for these oxides in the cotunnite phase were initially found by minimizing energy, through atomic coordinates and cell relaxations. The Kohn–Sham eigenstates were expanded in a numerical orbitals basis set. Our calculations are based on extensive testings we previously developed with the SIESTA code [21] in HfO_2 phases utilizing different basis sets: double-zeta (DZ), double-zeta polarized (DZP), single-zeta (SZ) and single-zeta polarized (SZP) and with different degrees of atomic orbital confinement. In that work [21], the best compromise between precision and efficiency was found with the utilization of the SZ base in hafnia if it is combined with pseudopotentials in which metal atoms include partial core corrections. These findings also apply here to the ZrO_2 compound and in the case of Ti if its 3p electrons are included in the valence set. This SZ base and LDA have shown that they provide reliable results in the search of structural parameters as well as in relative energies in the treatment of polymorphic hafnia, zirconia and titania. A detailed study in HfO_2 polymorphs [21] shows its capabilities in the description of enthalpies and other structural parameters, e.g. atomic coordinates and cell parameters when compared to other first-principle calculations [22, 24]. In that study [21], and also found here, it shows that structural parameters (axes lengths and equilibrium volumes) and bulk modulus calculated in the *Pnma* phase using SIESTA with SZ and DZ basis sets differ by less than 1% and 3%, respectively. A uniform spatial grid equivalent to a plane wave cutoff energy of at least 900 eV was used here to project the charge density and calculate the exchange, correlation and Hartree potentials. All GGA calculations here shown are developed with the DZ basis set. Integrations in first BZ were performed using equi-spaced 50–75k-point grid.

The SIESTA method allows the calculations of total energies to be carried out in crystalline structures with arbitrary symmetries, and it includes stress tensor calculations, as detailed in [17].

In the present work, to obtain the nine independent C_{ij} elastic constants, the stress–strain curves were found in several crystallographic directions in the *Pnma* crystalline phase, using a set of strains as described in [25].

During the simulation, each stress–strain curve was determined by uniformly increasing the amount of deformation,

and allowing the relaxations of all internal atomic coordinates by means of the conjugate gradient (CG) technique.

The relaxation process was carried out until the forces on each atom and cell pressures were below 0.04 eV $Å^{-1}$ and 0.1 GPa, respectively. Each system was deformed starting from the minimum energy configuration. From our understanding, this is the first time that elastic constant determinations have been presented for the TiO_2 oxide in the *Pnma* phase with a first-principles method that utilizes a localized basis to represent the valence electrons. These elastic constants were previously estimated in ZrO_2 and HfO_2 with the empirical model potentials (EMP), fitted to elastic and vibrational properties of the three ambient pressure zirconia lattices by Mirgorodsky–Quintard [12], the ZrO_2-*Pnma* phase studied by Lowther [36] and we also show here an advance of the work [27] developed on TiO_2 with the accurate all-electron *ab initio* code NFP-LMTO [28, 29]. In this last case, the Ti atom was studied with the help of the frozen overlapped core approximation (FOCA) approach, in which the $3p^6$ semicore electrons are kept frozen in the core while its wavefunction tails are allowed to interact with neighboring atoms. Therefore, $3s^2$, $3d^2$ electrons were included in the valence set. This electronic configuration was applied to the very well characterized TiO_2 in the fundamental rutile structure, and it was shown to be a proper selection in the calculation of equilibrium volume, lattice constants, elastic stiffnesses and bulk modulus. These physical constants are in agreement with theoretical and experimental values (see [33] and references therein). Extensive studies on TiO_2 by Muscat *et al* [33] have shown that its structural parameters are well accounted for with all-electron linear combination of atomic orbitals and LDA (CRYSTAL-98 code, LCAO-LDA) as well as pseudopotentials, plane waves and LDA approximations (PW-LDA), if, in the case of the utilizations of the Ti pseudopotential, short core Ti atoms are utilized. Our tests of SIESTA-LDA in the TiO_2 rutile structure have shown that **a**, **b**, **c** cell parameters and bulk modulus agree with previous accurate *ab initio* calculations to 1% (cell axes) and 5%, respectively. The utilization of NFP-LMTO-LDA code improves a little, providing 0.5% and about +5% accuracy with respect to **a**, **b** and **c** at $B = 230$ GPa measured by neutron diffraction and x-ray methods [34], respectively.

3. Procedure for the elastic constant determinations

The orthorhombic *Pnma* phase, denoted cotunnite, belongs to the group IV-B oxides and has three lattice parameters a, b and c, with Bravais lattice vectors $(a, 0, 0)$, $(0, b, 0)$ and $(0, 0, c)$. This structure is shown in figure 1. By applying a small set of deformations, the stress components directly calculated by the code are associated with the corresponding stress components determined by the linear relation between stress–strain provided by the elasticity theory.

The stress tensor components are related to the strain tensor elements through the generalized Hooke's law, which can be expressed as [30]

$$\sigma_{ij} = C_{ijkl}\varepsilon_{kl} \Rightarrow \sigma_i = C_{ij}\varepsilon_j \Rightarrow \vec{\sigma} = \widehat{C}\vec{\varepsilon}. \qquad (1)$$

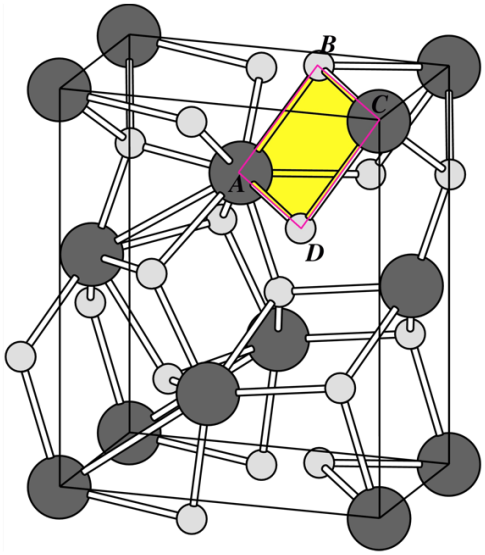

Figure 1. *Pnma* (cotunnite) unit cell. Dark gray balls denote metal atoms. A, B, C and D denote the atoms shown in charge density maps of figure 6.

(This figure is in colour only in the electronic version)

In the second equation we use Voigt's notation, replacing xx, yy, zz, yz, xz, xy by 1, 2, 3, 4, 5, 6, in which σ_i is a stress tensor element $i = 1 - 6$. ε_j is a strain tensor element $j = 1, 6$. C_{ij} is an elastic constant matrix element $i = 1, 6$; $j = 1, 6$.

The stiffnesses matrix of a orthorhombic system is given [31] by nine independent elastic constants:

$$C = \begin{bmatrix} C_{11} & C_{12} & C_{13} & 0 & 0 & 0 \\ & C_{22} & C_{23} & 0 & 0 & 0 \\ & & C_{33} & 0 & 0 & 0 \\ & & & C_{44} & 0 & 0 \\ & & & & C_{55} & 0 \\ & & & & & C_{66} \end{bmatrix}. \qquad (2)$$

The stiffness constants C_{11}, C_{22}, C_{33} are obtained by inducing uniaxial deformations to the crystalline axes **a**, **b**, **c**, respectively. To keep lattice anharmonicities low, seven to nine values of ε_i within the -0.02 to 0.02 range are used. Since $\sigma = C\varepsilon$, the C_{ij} are calculated by taking the linear part of a third-order polynomial used to fit the σ_i, ε_i data.

For this set of distortions, the volume does not stay constant and Hooke's law becomes as follows:

$$\sigma_1(\varepsilon_1) = C_{11}\varepsilon_1, \qquad \sigma_2(\varepsilon_2) = C_{22}\varepsilon_2, \qquad \sigma_3(\varepsilon_3) = C_{33}\varepsilon_3. \qquad (3)$$

For the following group of constants (C_{44}, C_{55}, C_{66}), we induce a set of shear deformations ε that maintain the volume, following [25, 35]. Under these conditions, Hooke's law becomes

$$\sigma_4(\varepsilon) = C_{44}\varepsilon_4. \qquad (4)$$

The last group of constants (C_{12}, C_{13}, C_{23}) are indirectly determined by applying constant volume deformations:

$$\sigma_1(\varepsilon) = C_{11}\varepsilon - C_{12}\varepsilon \qquad (5)$$

in which ε is an small deformation. C_{12} is obtained from equation (5) whereas C_{11} is calculated by the first equation of the set of equation (3).

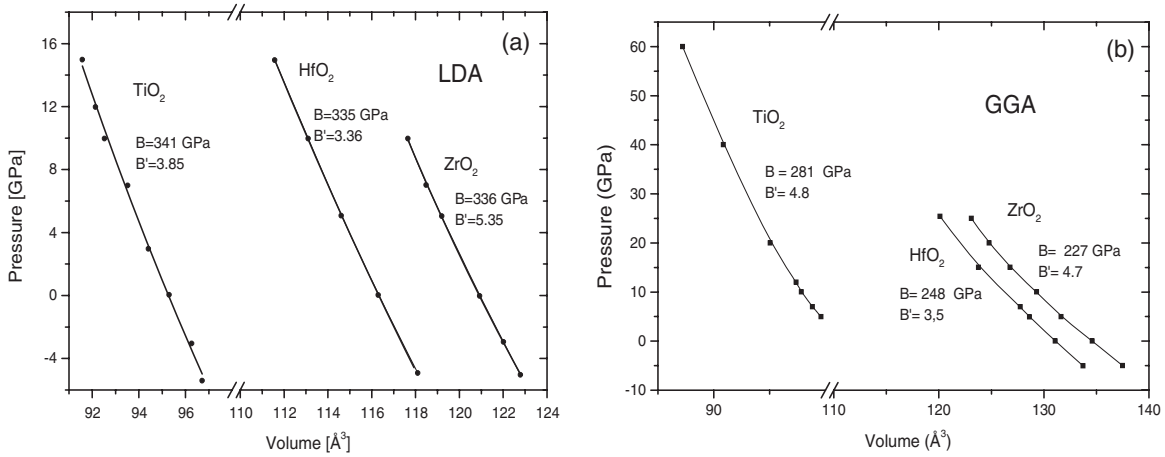

Figure 2. Pressure–volume relationships *ab initio* calculated with SIESTA code within the LDA and GGA approach. All cell parameters and atomic coordinates were relaxed after the application of pressure. Bulk moduli and its pressure derivatives were obtained by a fitting to a third-order P–V Birch–Murnaghan equation [39].

4. Simulation results and discussions: structural and elastic properties

In hafnia, the initial lattice parameters and atomic coordinates were taken from previous theoretical or available experimental data [36]. Then cell parameters and atomic coordinates are fully relaxed by the conjugate gradient technique. The final structural data are listed in tables 1, 2 and 3. The calculated volumes with LDA are 31.18, 30.22 and 23.81 Å^3 for HfO_2, ZrO_2 and TiO_2, respectively. In turn, the same values calculated with GGA are 32.07, 33.47 and 25.38 Å^3 for HfO_2, ZrO_2 and TiO_2, respectively. These values are close to the experimental ones and previous theoretical calculations with the state-of-the-art *ab initio* methods. As can be seen in tables 1, 2 and 3, our calculated volumes with SIESTA-LDA are in better agreement with experiments than those calculated with the SIESTA-GGA approach. In the case of TiO_2, our NFP-LMTO calculation gives an equilibrium volume of 23.24 Å^3, in slightly better agreement with respect to the experimental volume, 23.017 Å^3 ([26]).

In TiO_2, **a**, **b** and **c** axes calculated by the SIESTA-LDA approach, show good agreement (error bars below 2%) with experimental data (see table 1), although in this compound NFP-LMTO-LDA seems to be a better approximation (error bars below 1%). In turn, SIESTA-GGA provides increased **a** and **b** axes which depart by 4 and 5%, respectively, from experiments. Consequently, the equilibrium volume increases by about 10%. All calculated internal coordinates agree fairly well with experiments and previous calculations by Dewhurst and Lowther [26].

In ZrO_2, **a**, **b** and **c** axes' lengths and equilibrium volumes calculated with SIESTA-LDA show good agreement with available experimental data [4, 7] and previous theoretical assessments [36, 26, 37] (table 2). Although our equilibrium volume calculated with GGA is increased by 10%, as the previous case of TiO_2, the internal atomic coordinates agree well with previous theoretical estimations (table 2).

In the last case of HfO_2, our calculated **a**, **b** and **c** axes' lengths and volumes with the SIESTA-LDA approach are in very good agreement with available experimental data [4, 38] as well as previous theoretical calculations [22, 37] (tables 1–3).

Table 1. Equilibrium structural parameters for $Pnma$-TiO_2.

Orthorhombic (TiO_2)	SIESTA-LDA	SIESTA-GGA	NFP LMTO[a]	LDA[b]	Experimental[c]
V_0(Å^3)	23.812	25.38	23.239	26.14	23.017
a (Å^3)	5.10	5.33	5.12	5.259	5.163
b(Å^3)	3.059	3.17	3.025	3.145	2.989
c(Å^3)	6.097	5.99	6.01	6.322	5.966
Ti(x)	0.274	0.238	0.244	0.2527	0.264
Ti(y)	0.25	0.25	0.25	0.25	0.25
Ti(z)	0.106	0.114	0.119	0.1063	0.1110
O_1(x)	0.365	0.366	0.36	0.3611	0.346
O_1(y)	0.25	0.25	0.25	0.25	0.25
O_1(z)	0.4125	0.431	0.428	0.4212	0.422
O_2(x)	0.027	0.041	0.027	0.0137	0.012
O_2(y)	0.75	0.75	0.75	0.75	0.75
O_2(z)	0.344	0.336	0.337	0.3472	0.325

[a] Reference [27].
[b] Reference [26].
[c] Reference [6] and references therein.

Elastic properties under hydrostatic pressures were also studied in detail with the SIESTA code and in the LDA and GGA approximations. In figure 2(a), we show the numerical pressure–volume curves for TiO_2, ZrO_2 and HfO_2, resulting from the application of pressures between −4 and 16 GPa, where cell parameters (angles and axes lengths), as well as internal atomic coordinates, were allowed to relax at each pressure. The data were fitted to a Birch–Murnaghan third-order nonlinear P–V equation ([39]) which provides the following bulk moduli B_0 and pressure derivatives B_0': B_0 = 341 GPa, 335 GPa and 336 GPa, and $B_0' = 3.85$, 3.36 and 5.35 for TiO_2, HfO_2 and ZrO_2, respectively.

In figure 2(b), the pressure–volume relations are shown. They are calculated using similar procedures to figure 2(a), but with the GGA approach. In this case, we found changes in the

Table 2. Equilibrium structural parameters for *Pnma*-ZrO_2.

Orthorhombic (ZrO_2)	SIESTA-LDA	SIESTA-GGA	GGA[a]	LDA[b]	LDA[c]	Experimental[d]	Experimental[e]
V_0(Å^3)	30.225	33.47	30.859	29.4125	30.57	30.58	30.16
a(Å^3)	5.61	5.77	5.61	5.71	5.59	5.620	5.5873
b(Å^3)	3.285	3.45	3.347	3.25	3.34	3.347	3.3298
c(Å^3)	6.55	6.71	6.5658	6.34	6.55	6.503	6.4847
Zr(x)	0.247	0.246	0.246	0.251	0.247	0.262	
Zr(y)	0.25	0.25	0.25	0.250	0.25	0.250	
Zr(z)	0.113	0.112	0.113	0.109	0.118	0.109	
O_1(x)	0.3633	0.360	0.36	0.364	0.360	0.35	
O_1(y)	0.25	0.25	0.25	0.250	0.25	0.25	
O_1(z)	0.421	0.426	0.425	0.422	0.429	0.45	
O_2(x)	0.030	0.0264	0.024	0.021	0.028	0.04	
O_2(y)	0.75	0.75	0.75	0.75	0.75	0.75	
O_2(z)	0.335	0.34	0.338	0.328	0.333	0.33	

[a] Reference [37].
[b] Reference [36].
[c] Reference [26].
[d] Reference [7].
[e] Reference [5].

Table 3. Equilibrium structural properties of HfO_2 in the *Pnma* phase.

Orthorhombic (HfO_2)	SIESTA-LDA	SIESTA-GGA	GGA[a]	LDA[b]	LDA[c]	Experimental[d]	Experimental[e]
V_0(Å^3)	29.05	32.07	29.732	29.89	30.66	29.652	29.68
a(Å^3)	5.55	5.66	5.553	5.557	5.48	5.5544	5.55
b(Å^3)	3.25	3.39	3.302	3.293	3.35	3.3070	3.311
c(Å^3)	6.44	6.67	6.4842	6.531	6.68	6.4572	6.461
Hf(x)	0.247	0.247	0.246	0.245	0.249	0.2461	
Hf(y)	0.25	0.25	0.25	0.25	0.25	0.25	
Hf(z)	0.113	0.115	0.112	0.115	0.115	0.1104	
O_1(x)	0.360	0.346	0.359	0.359	0.360	0.3591	
O_1(y)	0.250	0.250	0.25	0.250	0.250	0.25	
O_1(z)	0.426	0.431	0.426	0.426	0.425	0.4256	
O_2(x)	0.022	0.016	0.024	0.025	0.022	0.0245	
O_2(y)	0.75	0.75	0.75	0.750	0.750	0.75	
O_2(z)	0.339	0.347	0.339	0.337	0.339	0.3388	

[a] Reference [37].
[b,c] Reference [22] and references cited therein.
[d] Reference [5].
[e] Reference [38].

calculated bulk moduli, which drop to $B_0 = 281$ GPa, 248 GPa and 227 GPa in TiO_2, HfO_2 and ZrO_2, and $B_0' = 4.8$, 3.5 and 4.7 for TiO_2, HfO_2 and ZrO_2, respectively. All cases were least-squares fitted to a third-order Birch–Murnaghan equation of state [39].

The GGA approximation was used to calculate the structural parameters and the compression modulus for comparison purposes. In this case, overestimation of the structural parameters and an underestimation of the compression moduli were found in ZrO_2, HfO_2 and TiO_2 with respect to the present and other LDA calculations [21, 22, 37, 40].

Elastic constant results are shown in table 4. In titania, zirconia and hafnia, it is found that the uniaxial elastic constants increase noticeably with respect to the corresponding normal phases. In TiO_2, for instance, comparing our theoretical cotunnite structure (LDA) with experimental rutile [41], we find that $C_{11}^{\mathrm{LDA}} = 688$ GPa exceeds significantly $C_{11}^{\mathrm{Rut}} = 268$ GPa, while $C_{33}^{\mathrm{LDA}} = 649$ GPa is much greater than $C_{33}^{\mathrm{Rut}} = 484$ GPa. For ZrO_2, on the other hand, our $C_{11}^{\mathrm{LDA}} = 618$ GPa again exceeds the monoclinic (Mon) experimental value $C_{11}^{\mathrm{Mon}} = 361$ GPa, $C_{22}^{\mathrm{LDA}} = 510$ GPa is greater than $C_{22}^{\mathrm{Mon}} = 408$ GPa, while $C_{33}^{\mathrm{LDA}} = 649$ GPa doubles $C_{33}^{\mathrm{Mon}} = 258$ GPa. However, shear moduli are larger but not quite different with respect to the normal phases. In TiO_2, the calculated $C_{44}^{\mathrm{LDA}} = 129$ GPa is slightly greater than $C_{44}^{\mathrm{Rut}} = 124$ GPa, while $C_{66}^{\mathrm{LDA}} = 204$ GPa is close to $C_{66}^{\mathrm{Rut}} = 190$ GPa. In ZrO_2 $C_{44}^{\mathrm{LDA}} = 99$ GPa equals $C_{44}^{\mathrm{Mon}} = 99$ GPa, $C_{55}^{\mathrm{LDA}} = 178$ GPa doubles $C_{22}^{\mathrm{Mon}} = 81$ GPa, while $C_{66} = 174$ GPa exceed $C_{66}^{\mathrm{Mon}} = 126$ GPa (see [12, 41, 42]). We have to recall that uniaxial elastic constants are related to compound ionicity and the number of oxygen atoms surrounding each metal ion [25]. In HfO_2 and ZrO_2, the coordination of the normal, monoclinic $P2_1/c$ phase is 7

Table 4. Calculated elastic constants of group IV-B: TiO_2, HfO_2, ZrO_2 oxides in the *Pnma* symmetry, compared with other LDA calculations and model potential.

	Titania TiO_2			Zirconia ZrO_2			Hafnia HfO_2		
Elastic constants (GPa)	SIESTA LDA	SIESTA GGA	NFP-LMTO[a]	SIESTA LDA	PP-PAW LDA[b]	Model pot. EMP[c]	SIESTA LDA	SIESTA GGA	Model pot. EMP[c]
C_{11}	688	619	646	619	474	463	664	502	477
C_{22}	510	350	475	450	348	400	575	261	415
C_{33}	649	282	635	632	314	429	640	597	446
C_{12}	258	218	250	176	164	165	193	122	172
C_{13}	240	178	229	210	201	193	236	159	202
C_{23}	253	82	283	224	149	249	235	244	151
C_{44}	129	52	148	107	68	31	137	78	31
C_{55}	133	43	203	178	114	113	185	90	117
C_{66}	204	219	246	174	132	126	165	111	132

[a] Present work.
[b] PP-PAW [1].
[c] Empirical model potential [12].

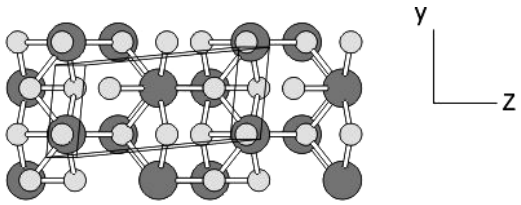

Figure 3. Primitive cell subjected to ε_4 shear deformation, side view. Dark gray circles denote metal atoms.

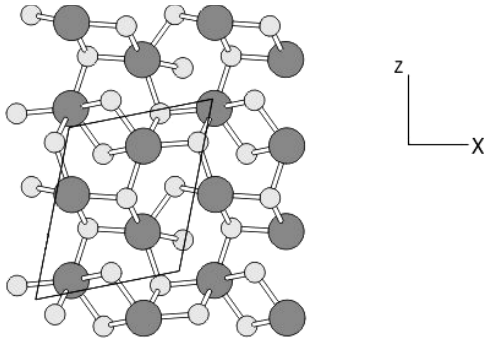

Figure 4. Primitive cell under ε_5 shear deformation, side view.

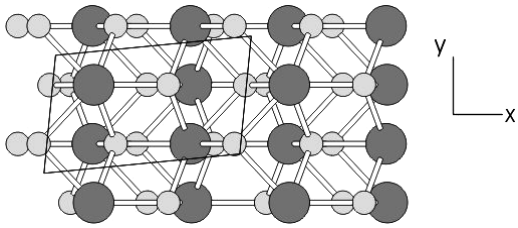

Figure 5. Primitive cell under ε_6 shear deformation, side view.

while in TiO_2, rutile structure, it is 6. Both structures increase its bulk modulus when transformed to the compact, high density, cotunnite phase, in which the coordination is 9. Since the bulk modulus B_0 depends on uniaxial and biaxial stiffness constants (see the first of equations (6)), high values for C_{11}, C_{22} and C_{33}, and in C_{12}, C_{13} and C_{23} constants, will determine a high resistance to volume deformation under hydrostatic compression in this phase.

Since the elastic constants corresponding to shear strains (see figures 3–5) do not increase in value in this high density phase, this behavior can be seen as increased anisotropy found in the present system, with orthorhombic symmetry (see figure 1)

Since monocrystalline samples are difficult to grow in the sizes necessary for accurate elastic constant C_{ij} measurements, there is a shortage of information about them in these high density phases. On the other hand, experimental results for bulk moduli can be found, as well as the lattice parameters and atomic positions.

Considering that a polycrystalline aggregate is a set of simple monocrystals with a random orientation, the determination of the stress–strain function can be established in two extreme cases: by equating any uniform strain in the polycrystalline aggregate to the external strain value or by equating the uniform stress to the external stress. The first scheme is called the Voigt approximation [14] and the latter is the Reuss approximation [15].

By applying these maximum and minimum cases to our orthorhombic crystals, an intermediate case can provide results that are in better agreement with experiments, as done in [25]. Following the methodologies of the cited work along with energy considerations from Hill [16] for which Voigt and Reuss equations represent upper and lower bounds of polycrystalline elastic properties, the bulk modulus B_0 and the shear modulus G_0 were estimated as an arithmetic mean of these extremes:

$$9B_V = (C_{11} + C_{22} + C_{33}) + 2(C_{12} + C_{13} + C_{23})$$

$$15G_V = (C_{11} + C_{22} + C_{33}) - (C_{12} + C_{13} + C_{23}) + 3(C_{44} + C_{55} + C_{66})$$

$$1/B_R = (S_{11} + S_{22} + S_{33}) + 2(S_{12} + S_{13} + S_{23})$$

$$15/G_R = 4(S_{11} + S_{22} + S_{33}) - 4(S_{12} + S_{13} + S_{23}) + 3(S_{44} + S_{55} + S_{66})$$

Table 5. Theoretical mean values of compression moduli B_0, shear elastic moduli G_0 and Young's moduli E_0 calculated with the Reuss–Voigt–Hill formula, the LDA and GGA approximations and compared with available data. All elastic moduli are expressed in GPa.

	TiO_2				ZrO_2		HfO_2	
Polycrystal	SIESTA LDA[a]	SIESTA GGA[a]	NFP-LMTO LDA[a]	FP-LMTO LDA[b]	SIESTA LDA[a]	PP-PAW LDA[c]	SIESTA LDA[a]	SIESTA GGA[a]
B_0^{th}	370	221	362	386 ± 10	320	254	354	246
B_{exp}			431[b]		332[d], 296[e], 278[f]		340[g], 312[h]	
G_0^{th}	162	96	163	—	160	112	176	103
E_0^{th}	424	251	425	—	411	293	453	271

[a] Present work.
[b] Reference [6].
[c] Reference [1].
[d] Reference [4].
[e] Reference [9].
[f] Reference [10].
[g] Reference [7].
[h] Reference [11].

$$B_0 = B_H = \frac{(B_V + B_R)}{2} \qquad G_0 = G_H = \frac{(G_V + G_R)}{2} \tag{6}$$

in this case, S_{ij} are elastic compliances, while subscripts V, R, H denote Voigt, Reuss, Hill approaches. Young modulus and Poisson coefficient were determined using the following relations [32]:

$$E = \frac{9B_0G_0}{3B_0 + G_0} \qquad \nu = \frac{3B_0 - 2G_0}{2(3B_0 + G_0)} \tag{7}$$

in which E is the Young's modulus and ν is the Poisson coefficient.

In table 5, mean values of shear elastic moduli and bulk moduli with the previously mentioned approximations are shown compared to experimental results and values obtained with other theoretical methods. All of our values are assessed with the polycrystalline approach.

Calculated bulk moduli B_0 using SIESTA and the polycrystalline approximations were: 370, 320 and 354 GPa for TiO_2, ZrO_2 and HfO_2, respectively, and similar theoretical values for single crystals, and calculated with pressures of 341, 335 and 336 GPa for TiO_2, ZrO_2 and HfO_2, respectively. These theoretical values are to be compared with $B_0^{exp} = 431$ GPa for TiO_2 [6], $B_0^{exp} = 278$–332 GPa for ZrO_2 [4, 5, 10, 11] and $B_0^{exp} = 312$–340 GPa for HfO_2 [5, 7–9]. In turn, our NFP-LMTO code provides $B_0^{th} = 362$, for TiO_2, which is slightly below previous calculations by another similar code, $B_0^{th} = 386$ GPa [6]. However, our $B_0^{th} = 221$ GPa calculated with SIESTA-GGA is much lower than all mentioned theoretical assessments.

Considering that the shear modulus represents the resistance to plastic deformation while the bulk modulus represents resistance to fracture, a high (low) B/G value is associated with ductility (brittleness). A critical value for the ductile–brittle transition can be seen in [43] and corresponds to a value of 1.75. The values obtained here with SIESTA and LDA are 2.28, 1.92 and 2.01 for titania, zirconia and hafnia, respectively. Similar values were obtained for TiO_2 with SIESTA-GGA: 2.3 and with NFP-LMTO-LDA: 2.22. However, note that, with SIESTA-GGA, B_0 and G_0 are underestimated.

5. Elastic anisotropies

It is well known that induced micro-fractures in ceramics are due to the anisotropic thermal expansion coefficient as well as the elastic anisotropy. In structural oxides, the elastic anisotropy is important in understanding the elastic properties, hoping to find the mechanisms to improve on their durability. All the known single crystals are essentially elastically anisotropic, and an appropriate description of such behavior is therefore important in science and engineering as well as crystal physics. The shear anisotropic factor for the {100} shear planes between the ⟨011⟩ and ⟨010⟩ directions is defined as [25]

$$A_1 = \frac{4C_{44}}{C_{11} + C_{33} - 2C_{13}}. \tag{8}$$

For the {010} shear planes between ⟨101⟩ and ⟨001⟩ directions it is

$$A_2 = \frac{4C_{55}}{C_{22} + C_{33} - 2C_{23}} \tag{9}$$

and for the {001} shear planes, between ⟨110⟩ and ⟨010⟩ directions it is

$$A_3 = \frac{4C_{66}}{C_{11} + C_{22} - 2C_{12}} \tag{10}$$

in which the value of one indicate an elastic isotropy, and any departure from unity corresponds to a certain degree of elastic anisotropy.

For all of them, SIESTA shows that the most pronounced anisotropy coefficient was found to be A_1, which is, in all systems, close to one-half. This case corresponds to strains of the ε_4 type, related to {100} slide planes where the elastic constant is weak, as shown in figure 3. Since A_2 and A_3 are closer to unity, all crystals are less anisotropic in that case.

Table 6. Shear anisotropic factors for group IV-B oxides calculated with LDA and GGA approaches.

	TiO_2		ZrO_2	HfO_2	
Constants	SIESTA LDA	NFP-LMTO LDA	SIESTA LDA	SIESTA LDA	SIESTA GGA
A_1	0.60	0.72	0.52	0.66	0.40
A_2	0.81	1.49	1.13	0.99	0.97
A_3	1.20	1.59	0.94	0.77	0.86

In TiO_2, we have performed a similar LDA calculation with the all-electron NFP-LMTO code, in which the core of both Ti and O atoms are treated in different ways with respect to the pseudopotential approach. In this last case, the core electrons of the Ti atom are kept frozen and allowed to overlap with neighboring atoms (FOCA approach). We have found good agreement between both methods, SIESTA and NFP-LMTO: table 4 shows that uniaxial and biaxial elastic constants agree (in a 10% error bar) although for shear elastic constants C_{55} and C_{66} the differences are more pronounced. In spite of this, table 5 shows remarkable agreement between the averaged values of B_0^{th}, G_0^{th} and E_0^{th} for both methods. However, the difference in G_0^{th} is amplified in the shear anisotropy factors shown in table 6. Therefore, extreme care has to be taken in this case and should need revision in future work.

In a cubic crystal, the linear bulk modulus is the same for all directions and therefore only the shear anisotropy is enough to describe the elastic anisotropy. However, in the orthorhombic crystal, the elastic anisotropy arises from the linear bulk anisotropic modulus added to the anisotropic shear. The anisotropy in bulk modulus along the **a** axis (B_a) and the **c** axis B_c with respect to **b** (B_b) can be expressed as

$$A_{B_a} = \frac{B_a}{B_b} = \alpha \qquad \text{and} \qquad A_{B_c} = \frac{B_c}{B_b} = \frac{\alpha}{\beta} \quad \text{respectively} \tag{11}$$

where α and β are constants defined as

$$\alpha = \frac{(C_{11}-C_{12})(C_{33}-C_{13}) - (C_{23}-C_{13})(C_{11}-C_{13})}{(C_{33}-C_{13})(C_{22}-C_{12}) - (C_{13}-C_{23})(C_{12}-C_{23})}$$
$$\beta = \frac{(C_{22}-C_{12})(C_{11}-C_{13}) - (C_{11}-C_{12})(C_{23}-C_{12})}{(C_{22}-C_{12})(C_{33}-C_{13}) - (C_{12}-C_{23})(C_{13}-C_{23})}. \tag{12}$$

The compressibility anisotropy factors along crystallographic axes are shown in table 7 and have been calculated from equations (11) where α and β are defined in equation (12). It should be noted that any departure from unity again corresponds to a degree of elastic anisotropy. In this case, the largest anisotropy factors correspond to titania and zirconia.

6. Thermoelastic properties

The Debye temperature is an important physical parameter in solids because it defines a temperature scale for atomic vibrations and it is related to the solid sound speed, too. One common method for the calculation of the Debye temperature (θ_D) comes from the knowledge of the elastic properties of the material, which is employed to calculate the mean sound velocity v_m and then θ_{Dp}:

Table 7. Anisotropy factor values for hydrostatic compressions along crystallographic axes. The two columns are calculated from equations (11) and (12).

	A_{B_a} (α)	A_{B_c} (β)
TiO_2	1.650	1.480
ZrO_2	1.640	1.630
HfO_2	1.235	1.330

$$\theta_{Dp} = \frac{\hbar}{k_B}\left[\frac{6\pi^2 N}{V_0}\right]^{1/3} v_m \tag{13}$$

in which $\hbar = h/2\pi$, h = Planck's constant, k_B = Boltzmann's constant, N = ions number in the unit cell, V_0 = equilibrium volume, v_m = mean value of the sound speed, which is defined by

$$v_m = \left[\frac{1}{3}\left(\frac{2}{v_t^3} + \frac{1}{v_l^3}\right)\right]^{-\frac{1}{3}} \tag{14}$$

in which v_l and v_t are the lattice wave velocities with longitudinal and transverse polarizations, respectively. They are calculated by the Navier equations from the knowledge of the shear modulus average G_0 and bulk modulus B_0:

$$v_t = \sqrt{\frac{G_0}{\rho}}, \qquad v_l = \left[\frac{(B_0 + \frac{4}{3}G_0)}{\rho}\right]^{1/2}. \tag{15}$$

Since the LDA approach slightly underestimates the equilibrium cell volume, the mass density is therefore larger and the resulting sound speed is slightly increased. The obtained values of the polycrystal Debye temperature calculated with equation (13) is 897 K for titania, certainly above the measured value of 790 K for the rutile phase [44] (this is reasonable because of the higher mass density and stiffer *Pnma* phase compared with rutile), while for HfO_2 and ZrO_2 we have calculated 549 K and 695 K, respectively. Predicted sound velocity values together with Poisson coefficients and Debye temperatures are shown in table 8. In this table, we also included similar values that we calculated with the all-electron method NFP-LMTO [28, 29].

The high value of Poisson constant ν is associated with the increased importance of two-body interatomic forces, compared to three-body terms, corresponding to bending forces which are typical of covalent bonds. In HfO_2, GGA [22] and the model potential [12] give values of $\nu = 0.32$ and 0.34, respectively, which are higher than $\nu = 0.286$ given by LDA, which indicates that LDA-SIESTA enhances the covalent bonds and their interaction. Figures 6 and 7 show the electronic charge density differences between LDA and GGA approaches. Electronic densities around oxygen atoms are more elongated towards metal ions in LDA (figure 6) than the almost symmetric density provided by GGA. Besides, certain covalent interactions between neighboring oxygen atoms can be seen. From tables 4, 5 and 8 we found

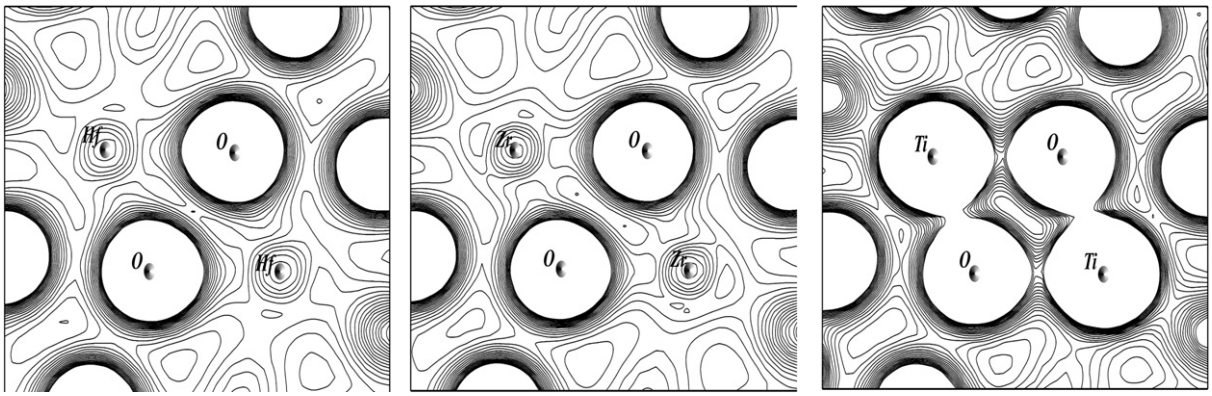

Figure 6. Pseudo valence charge densities contour map of HfO_2, ZrO_2 and TiO_2 with LDA, which correspond to the plane containing the four atoms A, B, C and D of figure 1. Contour step is equal to 0.005 electrons Å^{-3} and charge densities inside oxygen and Ti atoms are not shown, because they are cut above 0.1 electrons Å^{-3}.

Table 8. Calculated Poisson coefficients, transverse, longitudinal mean sound speeds and Debye temperatures θ_D for group IV-B oxides of the polycrystal. Unless noted, all calculations were done with LDA.

	TiO_2			ZrO_2	HfO_2		
Properties	SIESTA		NFP-LMTO[a]	SIESTA	SIESTA	SIESTA-GGA	EMP[b]
ν	0.31		0.304	0.27	0.288	0.32	0.34
v_t (m s^{-1})	5436		5350	4985	3999	3215	2815
v_t (m s^{-1}) exp[c]		5500					
v_l (m s^{-1})	10 327		10 078	9016	7339	6229	5717
v_l (m s^{-1}) exp[c]		10 300					
v_m (m s^{-1})	6078		5976	5554	4461	3599	3161
v_m (m s^{-1}) exp[c]		6900					
θ_D (K)	904		899	765	603	483	306
θ_D (K) exp[c]		790					

[a] Reference [27].
[b] Empirical model potential, see [12].
[c] Measurements in rutile [44].

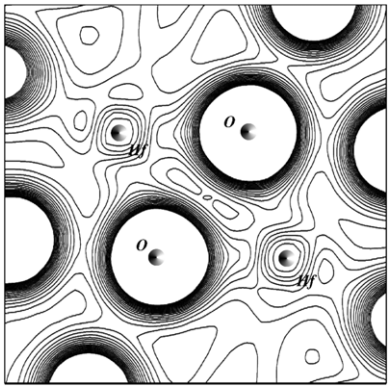

Figure 7. An example of pseudo valence charge densities contour map of HfO_2 calculated with SIESTA-GGA, which corresponds to the plane containing the four atoms A, B, C and D of figure 1. Contour steps are equal to 0.005 electrons Å^{-3} and charge densities inside oxygen atoms are not shown, for example, because they are cut above 0.1 electrons Å^{-3}.

a remarkable agreement in the elastic properties between SIESTA and NFP-LMTO in TiO_2. Both methods give very similar elastic constants, sound speeds and Debye temperatures. Covalent bonds can be seen in figure 6, in which the anisotropic shape of oxygen atoms comes from their sp hybrids pointing towards neighboring metal atoms. This shape in the electronic distribution somewhat explains the high value of shear moduli compared to pure ionic compounds. In terms of interatomic potentials, this covalency increases the magnitude of three-body terms, bending stiffness and shear modulus and consequently reduces the Poisson coefficient. We have to recall that pure ionic compounds, like KCl for instance, show a very low shear modulus, and C_{12} almost equal to C_{44}, satisfying the Cauchy relation $C_{12} = C_{44}$, which is based on a model where bending forces are neglected. On the other hand, for comparison, we mention that the Au metal shows a high Poisson coefficient (0.42), a fact that gives to this material a very malleable behavior. In contrast, the excellent covalent material, diamond, shows a small Poisson coefficient of 0.14. If we take the average between these extreme cases, we get a value of $\eta = 0.28$, which gives $B/G = 1.75$, the recognized boundary value between brittle and ductile behavior.

Charge transfer from Ti to oxygen atoms (given by the modified Mulliken populations, $\delta Q_O = -0.63$ and $\delta Q_{Ti} = 1.3$ in units of $|e|$) is consistent with the electronegativity of

oxygen. This amount of charge transferred is similar in all materials studied here.

Since TiO_2 is the less studied material in the group in its *Pnma* phase, we complete the present description using the GGA-PBE approach implemented in SIESTA code. The elastic properties of TiO_2 inspected with this treatment for the electronic exchange correlation underestimate all elastic constants, with one exception, C_{66}. This is also seen in the bulk, shear and Young modulus, in which the averaged B_0 drops from 370 GPa (LDA) to 221 GPa (GGA), G_0 is lowered from 162 GPa (LDA) to 96 GPa (GGA) and the Young modulus E decays from 424 GPa (LDA) to 251 GPa (GGA). Averaged B_0 estimated with NFP-LMTO is 362 GPa which is somewhat closer to the 386 GPa found in previous FP-LMTO calculations ([6]). However, even when these LDA values are in an error bar of 20 GPa, all of them are more than 40 GPa below the measured $B_0 = 431$ GPa (and, because of this very high value, claimed to be the hardest known oxide) by Dubrovinsky *et al* [6]. The wide dispersion between theory and experiment suggests that a new measurement of the bulk modulus of *Pnma*-TiO_2, under extreme conditions may need to be performed.

7. Conclusions

We have studied the hardest phase (cotunnite) of the group IV-B oxides TiO_2, ZrO_2 and HfO_2. After the atomic positions and crystal axes parameters are *ab initio* fully relaxed with the SIESTA code, the stress tensor is calculated for a set of prescribed small distortions Then the components of the elastic constant tensor are determined. Most cases were studied with LDA and GGA-PBE approaches. To the best of our knowledge, there are no previous experimental data related to the measurement of the nine C_{ij} elastic constants of the *Pnma* structure. Therefore our values are a prediction. We also show here calculations of elastic constants of TiO_2-*Pnma*, with the NFP-LMTO and LDA to DFT. Structural and elastic properties of TiO_2 calculated with this all-electron method agree with the pseudopotential-based SIESTA code. Polycrystal elastic constants, like Young's modulus E, Poisson coefficients ν and bulk moduli B_0, are also estimated. We find in all materials that stiffnesses calculated with LDA are very high, Young's moduli are greater than 400 GPa and Poisson constants range between 0.27 and 0.30. This fact suggests that the mechanical properties of these oxides, in the cotunnite structure, have an intermediate behavior between brittle and ductile. These mechanical properties are similar, for instance, to cubic tungsten, which shows similar elastic constants and Poisson coefficients to the presently studied oxides. Therefore, the high bulk modulus B_0 together with the high shear modulus G_0 may suggest the possible utilization of these compounds as structural as well as dielectric materials.

The use of pseudopotentials and LDA approaches, in the three compounds, slightly underestimate lattice parameters, but give B_0 in fair agreement with available experimental data. In the case of ZrO_2, the theoretical averaged bulk modulus $B_0^{\mathrm{LDA}} = 320$ GPa is between the measured values of $B_0 = 278$ and 332 GPa. In contrast to this situation, calculations with GGA at $P = 0$ GPa overestimate lattice parameters but underestimate both B_0, G_0 and increase the values of the B/G quotient. Consequently, Poisson constant values are greater than 0.3. In this case, the resulting material is theoretically predicted to be more ductile than brittle. The underestimation of B_0 using GGA is of the order of 80–100 GPa, with respect to LDA and to experimental data but departures can be higher than 150 GP with respect to recent experiments at high pressures in TiO_2 [1]. Further, our charge density contour maps show that the present GGA description enhances the ionic character of the metal–oxygen bonds of the studied compounds. It is interesting to note that averaged values of B_0 in both LDA and GGA approaches predict that the stiffest material is TiO_2, followed by HfO_2 and ZrO_2, which coincides with experimental evidence.

Elastic anisotropies estimated with LDA under hydrostatic pressures show that **a** and **c** axes are stiffer than the **b** axis by 20–60%. This behavior is in agreement with recent measurements in ZrO_2 made by Ohtaka *et al* [11], where the **b** axis is more pressure-dependent than the **a** and **c** axes, respectively. Therefore, the ionic character for planes perpendicular to the **b** axis is greater than in the other two directions.

Thermoelastic properties like Debye temperature are also predicted, and can be considered of value for future research in the estimation of specific heat and atomic amplitude of vibration as a function of temperature. However, new experimental searches which attempt the determination of elastic constants, sound wave propagation speed and Debye temperatures for these compounds in the *Pnma* phase will be highly appropriate.

Acknowledgments

We would like to thank Oscar Lin for his help during manuscript preparation, as well as Secretaria de Ciencia y Tecnica, UNNE, for financial support to projects PI054/04 and PI068/07.

References

[1] Lowther J E 2006 *Phys. Rev.* B **73** 134110
[2] Ponce C A, Casali R A and Caravaca M A 2008 *J. Phys.: Condens. Matter* **20** 45213
[3] Jayaraman A, Wangand S Y and Sharma S K 1993 *Phys. Rev.* B **48** 9205
[4] Haines J, Léger J M and Atouf A 1995 *J. Am. Ceram. Soc.* **78** 445
[5] Haines J, Léger J M, Hull S, Petitet J P, Pereira A S, Perottoni C A and da Jornada J A H 1997 *J. Am. Ceram. Soc.* **80** 1910
[6] Dubrovinsky L S, Dubronvinskaia N A, Swamy V, Muscat J, Harrison N M, Ahuja R, Holm B and Johansson B 2001 *Nature* **410** 653
[7] Degreniers S and Lagarec K 1999 *Phys. Rev.* B **59** 8467
[8] Ohtaka O, Fukui H, Kunisada T, Fujisawa T and Kikegawa T 2001 *Phys. Rev.* B **63** 174108
[9] Ohtaka O, Fukui H, Kunisada T, Fujisawa T, Funakoshi K, Utsumi W, Irifune T, Kuroda K and Kikegawa T 2001 *J. Am. Ceram. Soc.* **84** 1369

[10] Ohtaka O, Fukui H, Funakoshi K, Utsumi W, Irifune T and Kikegawa T 2002 *Int. J. High Pressure Res.* **22** 221
[11] Ohtaka O, Andrault D, Bouvier P, Schultz E and Mezouar M 2005 *J. Appl. Crystallogr.* **38** 727
[12] Mirgorodsky A P and Quintard P E 1999 *J. Am. Ceram. Soc.* **82** 3121
[13] Mattesini M, de Almeida J S, Dubrovinsky L, Dubrovinskaia N, Johanson B and Ahuja R 2004 *Phys. Rev.* B **70** 212101
[14] Voigt W 1928 *Lehrbuch der KrystallPhysik* (Leipzig: Teubner)
[15] Reuss A 1929 *Z. Angew. Math. Mech.* **9** 49
[16] Hill R 1952 *Proc. Phys. Soc.* A **65** 349
[17] Soler J M, Artacho E, Gale J D, Garcia A, Junquera J, Ordejon P and Sanchez-Portal D 2002 *J. Phys.: Condens. Matter* **14** 2745
[18] Perdew J P and Zunger A 1981 *Phys. Rev.* B **23** 5048
[19] Perdew J P, Burke K and Ernzerhof M 1996 *Phys. Rev. Lett.* **77** 3865
[20] Troullier N and Martins J L 1991 *Phys. Rev.* B **43** 1993
[21] Caravaca M A and Casali R A 2005 *J. Phys.: Condens. Matter* **17** 5795
[22] Kang J, Lee E C and Chang K J 2003 *Phys. Rev.* B **68** 54106
[23] Kleinman L and Bylander D M 1982 *Phys. Rev. Lett.* **48** 1425
[24] Zhao X and Vanderbilt D 2002 *Novel Materials an Processes for advanced CMOS: Proc. 2002 MRS Fall Mtg* vol 745 ed M I Gardner, J P María, S Stemmer and S de Gendt p 7.2.1
[25] Ravindran P, Fast L, Korzhavyl P A, Johansson B, Wills J and Eriksson O 1998 *J. Appl. Phys.* **84** 4891
[26] Dewhurst J K and Lowther J E 2001 *Phys. Rev.* B **64** 014104
[27] Casali R A, Ponce C A and Caravaca M A 2008 unpublished
[28] Methfessel M, van Shilfgaarde M and Casali R A 2000 *Electronic Structure and Physical Properties of Solids: the Use of the LMTO Method* (*Lecture Notes in Physics* vol 535) ed H Dreyssé (Berlin: Springer) p 114
[29] Bott E, Methfessel M, Krabs W and Schmidt P C 1998 *J. Math. Phys.* **39** 3393
[30] Nye J F 1957 *Physical Properties of Crystals* (London: Oxford University Press, Ely House)
[31] Musgrave M J P 1970 *Crystal Acoustics: Introduction to the Study of Elastic Waves and Vibrations in Crystals* (San Francisco, CA: Holden-Day)
[32] Landau L D and Lifshitz E M 1970 *Theory of Elasticity* (*Course of Theoretical Physics* vol 7) 3rd edn (Oxford: Butterworth-Heinemann)
[33] Muscat J, Swamy V and Harrison N M 2002 *Phys. Rev.* B **65** 224112
[34] Gerward L and Olsen J S 1997 *J. Appl. Crystallogr.* **30** 259
[35] Panda K B and Ravichandran K S 2006 *Acta Mater.* **54** 1641
[36] Lowther J E, Dewhurst J K, Leger J M and Haines J 1999 *Phys. Rev.* B **60** 14485
[37] Jaffe J E, Bachorz R A and Gutowski M 2005 *Phys. Rev.* B **72** 144107
[38] Liu L G 1979 *J. Phys. Chem. Solids* **41** 331
[39] Desgreniers S and Lagarec K 1999 *Phys. Rev.* B **59** 8467
[40] Zhao X and Vanderbilt D 2002 *Phys. Rev.* B **65** 233106
[41] Isaac D G, Cames J D, Anderson O L, Cynn H and Hake E 1997 *Phys. Chem. Minerals* **26** 31
[42] Fadda G, Truskinovsky L and Zanzotto G 2002 *Phys. Rev.* B **66** 174107
[43] Pugh S F 1954 *Phil. Mag.* **45** 823
[44] Wu A Y and Sladek R J 1982 *Phys. Rev.* B **25** 5230